Journal of Vacuum Science Technology B

An ultra-fast method for scanning tunneling spectroscopy

Hamed Alemansour,[1] S. O. Reza Moheimani,[1, a)] James H. G. Owen,[2] John N. Randall,[2] and Ehud Fuchs[2]
[1)]*Erik Jonsson School of Engineering and Computer Science, The University of Texas at Dallas, Richardson, TX 75080, USA*
[2)]*Zyvex Labs LLC, 1301 N Plano Rd., Richardson, TX 75081, USA*

Scanning tunneling microscope combines unique capabilities in imaging and spectroscopy with atomic precision and it can obtain energy-resolved spectroscopic data with atomic resolution. In this paper we utilize a recently proposed modification to the STM feedback control loop to acquire high quality d^2I/dV^2 images. We have developed a constant differential conductance imaging method by closing the STM feedback loop with a high precision dI/dV measurement. In this mode, the tip's vertical position is adjusted so as to keep the differential conductance constant during raster scanning of the surface. Based on this imaging mode, we propose a new technique to acquire fast and reliable scanning tunneling spectroscopy data simultaneously with the imaging.

I. INTRODUCTION

Scanning tunneling microscopy (STM) is based on maintaining a quantum tunneling current between a sharp conductive tip that is hovering within a sub-nanometer distance of a conductive sample[1,2]. To a first approximation, the STM image maps surface topographic features, however the local electronic properties of the sample can affect the tip height, so that the resulting image is in fact a mixture of topographic and electronic features. Early in the development of the STM, it was realised that the STM could be used to extract local electronic properties of surfaces, and various methods, collectively known as scanning tunneling spectroscopy (STS) have been designed for this specific purpose[3]. However, despite advancements in this field, there exist significant technical hurdles to increase the speed and precision of scanning tunneling spectroscopy techniques.

The electronic structure of a surface can be determined in several ways: the simplest involves performing successive constant-current imaging at different sample bias voltages[4–6]. Varying the bias voltage probes different surface states of the sample and can be used to map the spatial distribution of surface electronic states.

In many instances, however, a complete electronic structure map is not required and local measurements would be enough[7]. For these types of single-point spectroscopy, the STM tip is positioned over a specific point, the feedback loop is switched off, and the sample voltage is varied over the desired values, so as to acquire the tunneling current as a function of bias voltage, I(V). The bias voltage is then turned back to the previous constant-current imaging value and the feedback is reactivated. Similarly, the Local Density of States (LDOS) at a certain location can be determined from the differential conductance, dI/dV.

Current-imaging tunneling spectroscopy (CITS) is an extension of individual I(V) spectroscopy[8]. Tunneling spectra are taken at every pixel of an image. Spectroscopic information, e.g. current I(x,y) or differential conductance dI/dV maps at fixed bias voltages, are then produced from the corresponding data sets. This spectroscopy method requires pausing the scan and turning off the feedback loop for every pixel. This is a laborious task and a normal map of small sample area can take up hours[9]. Therefore, in this method low lateral drift and tip-sample junction stability are of key importance.

STM inelastic tunneling spectroscopy (STM-IETS) has been used to identify molecules on a conductive surface[10–12]. As the energy of tunneling electrons exceeds a threshold voltage, an inelastic channel for tunneling opens up in addition to the elastic tunneling current that can excite vibration of an atom or molecule on the surface. This is observed as an increase in the slope of the I-V curve, which is usually too small to be detected directly from dI/dV. This also appears as a peak or dip at a bias voltage corresponding to the energy of the vibrational mode in the d^2I/dV^2 signal and is measured by lock-in techniques. A small modulation voltage is added to the dc bias. The signal amplitude measured at twice the modulation frequency is proportional to d^2I/dV^2. This conventional way of measuring d^2I/dV^2 leads to a very small and noisy signal, even with the lock-in technique.

Previously, we demonstrated a method to improve the signal-to-noise ratio (SNR) of a differential conductance image by incorporating notch filters in the STM feedback loop[13]. We showed that this modified feedback loop enables us to apply a higher amplitude modulation without adversely affecting the topography measurements. In this paper, we employ the same method as in [14] to obtain a high SNR d^2I/dV^2 image. We expect these methods to benefit STM spectroscopic applications, enabling users to obtain reliable information about the local density of electron states (LDOS) of a sample and identify molecules or atoms on or beneath a surface. We also propose a method that the I-V curve can be obtained simultaneously with the topography image without interrupting the feedback loop. Similarly to CITS, our method also provides a tunneling spectra for every pixel of an images; however, it reduces the imaging time significantly.

The dI/dV image can be acquired simultaneously with the topography image by utilizing the modulation technique. This works by superimposing a sinusoidal modulation signal on the dc sample bias voltage and measuring the component of ac current that is in-phase with the modulation voltage[13,15]. For a small modulation amplitude, this signal is proportional to dI/dV. The feedback loop is closed on the dc tunneling current and the controller output constructs a constant-current topography image of the surface. Here, we propose the con-

[a)]Corresponding author: Reza.Moheimani@utdallas.edu

stant differential conductance imaging mode for STM. In this mode, the tip is scanned over the surface while the feedback loop keeps the component of current in-phase with the modulation constant.

The remainder of the paper continues as follows. In the next section, experimental setup and theoretical background are briefly explained. High signal-to-noise ratio d^2I/dV^2 imaging is presented in Section III. In Section IV, constant dI/dV imaging mode and its implementation are detailed. The ultra-fast current-voltage spectroscopy is explored in Section V, and the paper is concluded in Section VI.

II. EXPERIMENTAL METHODS

Experiments were performed using a home built room-temperature ultrahigh-vacuum scanning tunneling microscope with the base pressure of 10^{-11} Torr[16]. Real-time control tasks such as the STM feedback loop were handled by a ZyVector 20-bit digital control box[17]. We used Zurich Instruments HF2LI as an external lock-in amplifier and a FEMTO LCA-400K-10M as a transimpedance amplifier. The transimpedance amplifier has a bandwidth of 400 kHz with the amplification gain of 10^7.

We performed our experiments on hydrogen passivated Si(100)-2×1 samples. The ability to precisely pattern a hydrogen terminated silicon surface[14,18–20], selectively adsorb various atoms and molecules[21,22], and integrate new devices with conventional silicon electronics, make this surface ideal for developing atomically precise manufacturing methods. Our Si(100) samples are boron doped with a resistivity of 1 ohm cm. Tip and sample preparation procedures are reported in detail elsewhere[13,23].

Several methods have been proposed to approximate the current flowing through a tunneling junction (electrode-gap-electrode). In the energy-dependent approximation of the Bardeen model, the tunneling current is dependent on the density of states of the tip and the sample according to[24]:

$$I = \frac{4\pi e}{\hbar}\int_0^{eV} \rho_t(\varepsilon - eV)\rho_s(\varepsilon)T(\varepsilon,V,\delta)d\varepsilon \qquad (1)$$

where ρ_t, ρ_s, δ, and $T(\varepsilon,V,\delta)$ are the density of states of the tip, the density of states of the sample, the barrier thickness, and the transmission factor for tunneling from a tip to a sample state. Assuming that ρ_t and T are voltage independent[24], the first derivative of the tunneling current in Eq. 1 with respect to V results in the differential conductance dI/dV as follows:

$$\frac{dI}{dV} = \frac{4\pi e^2}{\hbar}\rho_t(0)\rho_s(eV)T(eV,V,\delta) \qquad (2)$$

Eq. 2 demonstrates that the differential conductance is proportional to the density of states of the sample.

In conventional STS, the current-voltage characteristic is recorded by keeping the tip at a fixed position over the surface and slowly sweeping the bias voltage. For a low frequency sweep, the measured current is primarily due to the quantum tunneling with the capacitive current being negligible. The

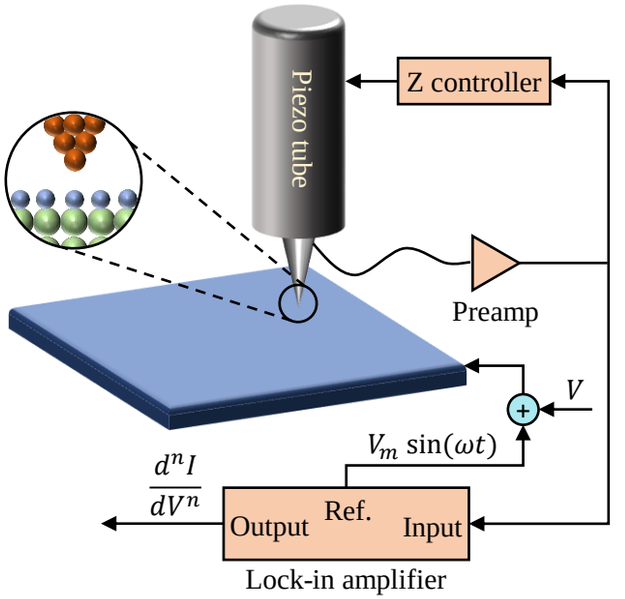

FIG. 1. Schematic representation of an STM operating in constant-current imaging mode. With the lock-in technique, d^nI/dV^n is measured at the sample bias voltage of V, simultaneously with imaging.

first derivative of the total current then provides information on LDOS of the surface, and the second derivative gives information on vibrations of the adsorbate.

Adding a dither voltage $V_m sin(\omega t)$ to the sample bias V will result in a tunneling current $I = f(V + V_m sin(\omega t))$. The Taylor series expansion of I around the voltage V is as follows:

$$\begin{aligned} I = f(V + V_m sin(\omega t)) &= \sum_{k=0}^{\infty} \frac{V_m^k}{k!}\frac{d^k f}{dV^k} sin^k(\omega t) \\ &= 1\left(f(V) + \frac{V_m^2}{4}\frac{d^2 f}{dV^2} + \frac{V_m^4}{64}\frac{d^4 f}{dV^4} + \dots\right) \\ &+ V_m sin(\omega t)\left(\frac{df}{dV} + \frac{V_m^3}{8}\frac{d^3 f}{dV^3} + \frac{V_m^5}{192}\frac{d^5 f}{dV^5} + \dots\right) \\ &- \frac{V_m^2}{4} cos(2\omega t)\left(\frac{d^2 f}{dV^2} + \frac{V_m^4}{12}\frac{d^4 f}{dV^4} + \dots\right) \\ &- \frac{V_m^3}{24} sin(3\omega t)\left(\frac{d^3 f}{dV^3} + \frac{V_m^5}{16}\frac{d^5 f}{dV^5} + \dots\right) \\ &+ \frac{V_m^4}{192} cos(4\omega t)\left(\frac{d^4 f}{dV^4} + \dots\right) \end{aligned} \qquad (3)$$

By grouping the terms with the same multiples of the modulation frequency, Eq. 3 can be written as

$$I = I_0 + \sum_{i=1}^{\infty}\left(a_{2i-1} sin((2i-1)\omega t) + a_{2i} cos(2i\omega t)\right). \qquad (4)$$

For a small dither voltage, the higher order terms of each group can be neglected and the amplitude of tunneling current at $n\omega$ is proportional to the n^{th} derivative of I, i.e.

$$a_i \propto \frac{d^n I}{dV^n} \qquad (5)$$

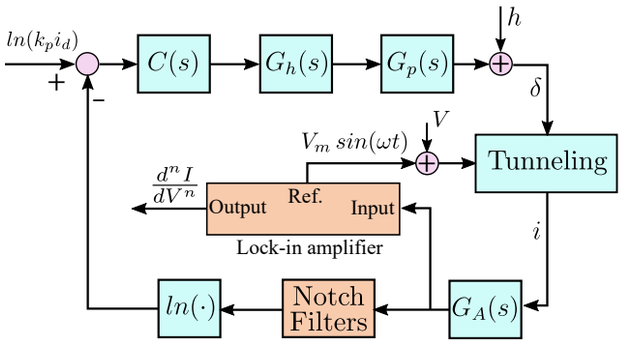

FIG. 2. The control block diagram of STM in constant-current mode. The tunneling current experiences a transient change when the tip encounters an unknown topographic feature, h, on the surface. The preamplifier $G_A(s)$ with the amplification gain of k_p converts the tunneling current to a measurable voltage. This is then regulated by the controller $C(s)$ through adjusting the tip-sample gap δ. The controller command is amplified by the high voltage amplifier $G_h(s)$, which drives the piezo actuator $G_p(s)$.

In practice, the n^{th} derivative of tunneling current at a fixed sample bias voltage is measured by a lock-in amplifier, as shown in Fig. 1. A sinusoidal modulation with the frequency of ω and amplitude of V_m is added to the dc bias voltage of sample. The resulting current is then sent back to the lock-in amplifier. For a low frequency dither signal, the capacitive component of total current is negligible and amplitude of the signal at $n\omega$ is proportional to $\mathrm{d^nI/dV^n}$. On the other hand, the capacitive component is substantial for a high frequency dither signal and it must be considered in the measurements. In this case, amplitude of the in-phase component of the total current at the fundamental frequency represents $\mathrm{dI/dV}$ and the quadrature part is proportional to the capacitance:

$$I_{total} = I + I_{cap} = I + CV_m\omega\, cos(\omega t) \tag{6}$$

where C is the total capacitance comprising the tip-sample and stray capacitances.

III. HIGH SNR dI / dV AND $\mathrm{d^2I/dV^2}$ IMAGING

In our previous work[13], we showed that high signal-to-noise ratio $\mathrm{dI/dV}$ images can be obtained by incorporating notch filters in the feedback loop. The modified STM feedback control system, depicted in Fig. 2, enables us to apply a higher amplitude dither voltage without adversely affecting the topography image, leading to a higher quality differential conductance image[25].

We use the same method to perform high SNR $\mathrm{d^2I/dV^2}$ imaging. Here, a 2 kHz dither signal is generated by the lock-in amplifier and added to the sample's - 2.5 V dc bias voltage. The amplified current is sent back to the lock-in amplifier to be compared with the reference signal. Total current, the in-phase component of current at the fundamental frequency, the quadrature component of current at the second harmonic, and the in-phase component of current at the third harmonic, are sent to ZyVector[17] for producing current, $\mathrm{dI/dV}$, $\mathrm{d^2I/dV^2}$, and $\mathrm{d^3I/dV^3}$ images, respectively.

The results are plotted in Fig. 3, where protrusions are white and depressions are black in the topography images. Similarly, regions of high current are white and regions of low current are black in the current images. Topography, $\mathrm{dI/dV}$, $\mathrm{d^2I/dV^2}$, and $\mathrm{d^3I/dV^3}$ images for a typical dither amplitude of 0.1 V are shown in Fig. 3 (a-d). The current setpoint is 1 nA in these experiments. The differential conductance and $\mathrm{d^2I/dV^2}$ images are quite noisy due to the low SNR.

For the second set of experiments, we incorporated notch filters in the feedback loop and imaged the same area. The center frequencies of these filters were located at the fundamental frequency of the dither voltage and the first four higher harmonics. The stop bandwidth of filters was 0.2 kHz. This modified feedback control system enabled us to apply a higher amplitude dither voltage, without adversely affecting the topography image in Fig. 3 (e). The quality of $\mathrm{dI/dV}$, $\mathrm{d^2I/dV^2}$, and $\mathrm{d^3I/dV^3}$ images are significantly improved as shown in Fig. 3 (f-h). Consequently, dimer rows and defects are clearly visible, whereas they are not in Fig. 3 (b-d). This method is, therefore, advantageous in detecting the location of buried dopants in a H-terminated silicon surface.

A Zurich instrument lock-in amplifier is used to demodulate the amplified current into the in-phase and 90°out of phase components at the fundamental frequency and higher harmonics. To measure the SNR of these signals, they were recorded with a sampling rate of 28.783 kHz at the output ports of the lock-in amplifier over 20 s time periods, while the lateral position of the STM tip was kept constant. The signal-to-noise ratio is defined as the ratio of the mean to the standard deviation of the signal. The SNR of $\mathrm{dI/dV}$, $\mathrm{d^2I/dV^2}$, and $\mathrm{d^3I/dV^3}$, were measured as 1.955, 0.094, and 0.002, respectively, with the conventional method and increased to 5.574, 4.393, and 1.046, with our method. These significant improvements in SNR were brought about by incorporating notch filters into the feedback loop, which allowed us to increase the modulation amplitude.

IV. CONSTANT DIFFERENTIAL CONDUCTANCE IMAGING

A simplified model of tunneling current between the sample and the tip of an STM can be expressed as[26,27]:

$$I \approx H(V,\rho_t,\rho_s)e^{-1.025\sqrt{\phi}\delta} \tag{7}$$

Constant current mode scanning tunneling microscopy is the most frequently used method for acquiring STM topography images. In this mode, a closed-loop control system adjusts the vertical position of the tip in order to keep the natural logarithm of tunneling current ($ln(I)$) constant. Assuming that all parameters except for δ are constant in Eq. 7, the tip-sample separation is linearly proportional to the $ln(I)$ of tunneling current.

From Eq. 7, the first derivative of I with respect to V is

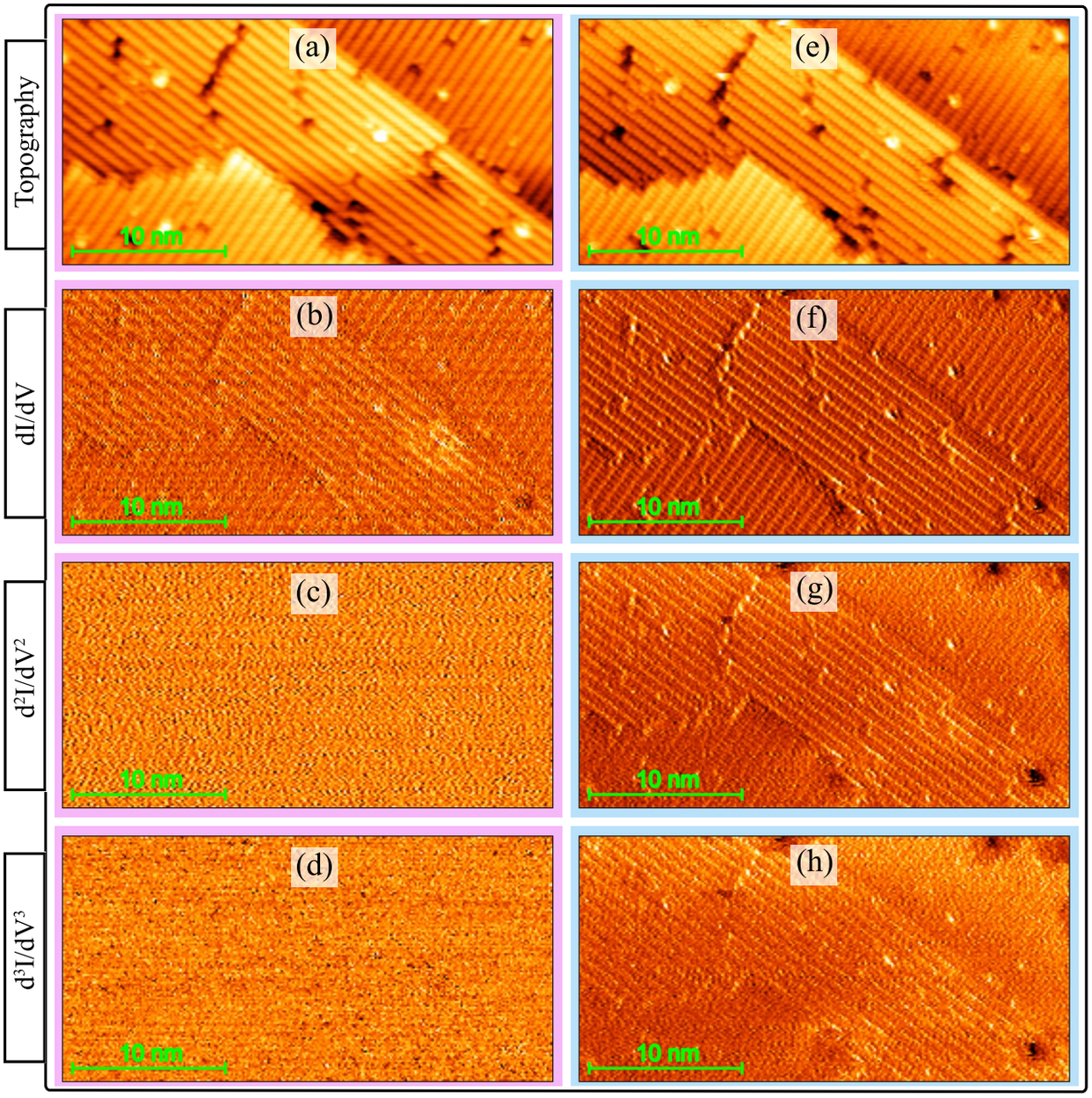

FIG. 3. Topography image (top row), dI / dV image (second row), d^2I/dV^2 image (third row), and d^3I/dV^3 image (bottom row) of a hydrogen terminated Si(100) surface. (a)-(d) with 0.1 V modulation amplitude and without notch filters in the feedback loop, (e)-(h) with 0.8 V modulation amplitude and with notch filters in the feedback loop.

expressed as:

$$\frac{dI}{dV} \approx \frac{dH}{dV} e^{-1.025\sqrt{\phi}\delta} \tag{8}$$

Under the same assumption as for the constant current mode imaging, Eq. 8 shows that $ln(dI/dV)$ is also linearly proportional to the tip-sample separation and can be used as a feedback signal.

Here, we close the STM feedback loop on the $ln(dI/dV)$ signal. This amounts to a new imaging mode for the UHV STM. The corresponding control system block diagram is shown in Fig. 4. A sinusoidal bias modulation with frequency of ω and amplitude of V_m is added to dc sample bias voltage. The resulting current is then amplified by the preamplifier and sent back to the lock-in amplifier that measures amplitude of the component of the current that is in-phase with the modulation signal (a_1 in Eq. 4). For a small dither voltage, a_1 is approximately proportional to dI / dV . This is then digitally scaled by k_l in the lock-in amplifier and sent to the ZyVector STM control system as an analog signal. The setpoint mi-

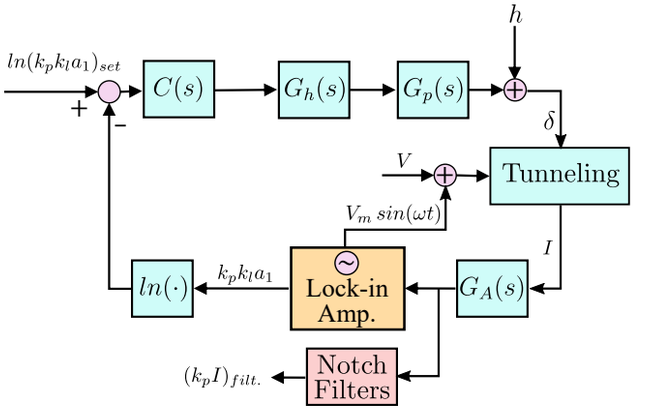

FIG. 4. The control block diagram of an STM in constant differential conductance mode. The modulation voltage $V_m sin(\omega t)$ is added to the sample bias voltage V. The resulted current is then amplified by the preamplifier $G_A(s)$. The lock-in amplifier measures the in-phase component of the amplified current, scales it by a factor of k_l, and sends it to the ZyVector for the control purposes.

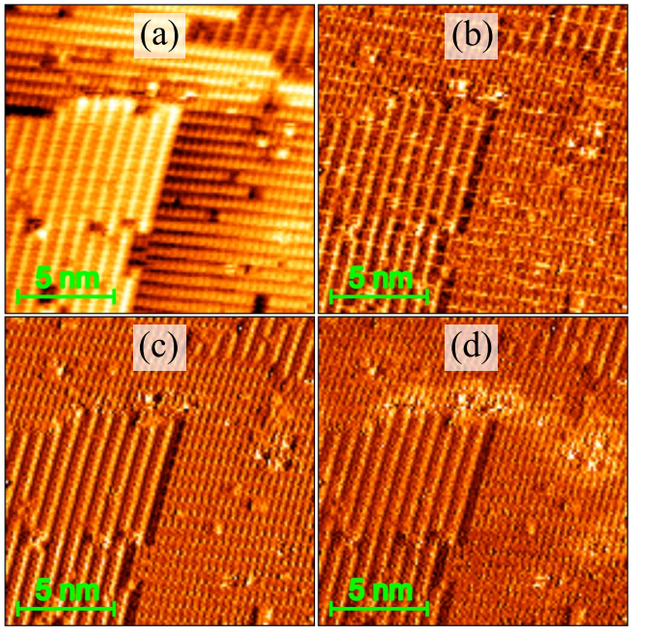

FIG. 5. (a) Topography image, (b) filtered dc current image, (c) dI/dV image, and (d) d^2I/dV^2 image of a Si(100)-2×1:H passivated surface, in constant differential conductance imaging mode. All of the images are obtained simultaneously.

nus the natural logarithm of this signal is defined as the error. The proportional integral controller regulates the tip-sample height in order to minimize the error signal. The controller output is then plotted along with the x and y positions of the tip to construct a topography image of the surface.

Fig. 5 shows images of a Si(100)-2×1:H passivated surface in constant differential conductance mode. All of the images were obtained simultaneously. A bias modulation at 2 kHz and amplitude of 0.8 V was added to - 2.5 V sample bias voltage. The topography image in Fig. 5 (a) is constructed by closing the feedback loop on $ln(k_pk_la_1)$, where a_1 is the amplitude of in-phase component of current with the modulation, k_p is the preamplifier gain of 10^7, and k_l is the lock-in amplifier scale factor of 10. The a_1 and a_2 images are also shown in Fig. 5 (c) and (d), respectively. It can be assumed that a_1 and a_2 are proportional to dI/dV and d^2I/dV^2, respectively. In this experiment, the setpoint $(a_1)_{set}$ was 0.1 nA. The image of dc tunneling current after the notch filters $(k_pI)_{filt.}$ is also shown in Fig. 5 (b).

V. ULTRA FAST CURRENT-VOLTAGE SPECTROSCOPY

In this section we introduce a new method to acquire complete I-V characteristics of a surface and the topography at the same time. This ultra-fast spectroscopy technique overcomes the slow speed inherent to the conventional scanning tunneling spectroscopy and allows real-space imaging of surface electronic states in real time. Many applications can be foreseen for this technology, e.g. we are using rapid spectroscopy to detect locations of buried dopants in silicon during atomic-scale device fabrication.

This method is based on the imaging mode explained in Sec. IV, with the difference that a high amplitude modulation voltage without a dc bias is applied to the sample. The feedback loop is then closed on the a_1 signal, i.e the fundamental frequency component of the tunneling current obtained from the lock-in amplifier. This provides the possibility to equally sweep both positive and negative voltages without the need to apply a very high amplitude modulation. A sinusoidal signal with the frequency of ω is applied to the sample. The resulting current contains both tunneling and capacitive components. A preamplifier, i.e. a transimpedance amplifier, converts the total current to a measurable voltage. This signal is then sent to the lock-in amplifier and is demodulated to the in-phase (a_1 in Eq. 4) and the quadrature components ($CV_m\omega$ in Eq. 6). The feedback loop is closed on the $ln(k_pk_la_1)$ signal when the surface is raster scanned. The tunneling current is obtained by subtracting the capacitive current, $CV_m\omega\,cos(\omega t)$, from the total current. This is recorded in conjunction with the modulation voltage to construct an I-V curve within a time span as short as the half period of the modulation. Also, the tunneling current image of choice at a fixed sample bias voltage between $-V_m$ and $+V_m$ can be constructed from the I-V curves data.

Fig. 6 shows simultaneously obtained images of a hydrogen passivated silicon surface with two adjacent depassivated dimer rows. The scan size is $16\,nm \times 16\,nm$ and the image size is 128×128 pixels. A sinusoidal voltage with a frequency of 2 kHz and amplitude of 2.5 V is applied to the sample. The topography image in Fig. 6 (a) is constructed by closing the feedback loop on $ln(k_pk_la_1)$. The a_1 image is shown in Fig. 6 (b). In this experiment, the setpoint $(a_1)_{set}$ is 0.1 nA. I-V curves are recorded simultaneously with the topography image for every pixel. There are 4600 Sa/nm with the Zurich instrument recording at a sampling rate of 460 kSa/s, the scan speed of 100 nm/sec, and the modulation frequency of 2 kHz.

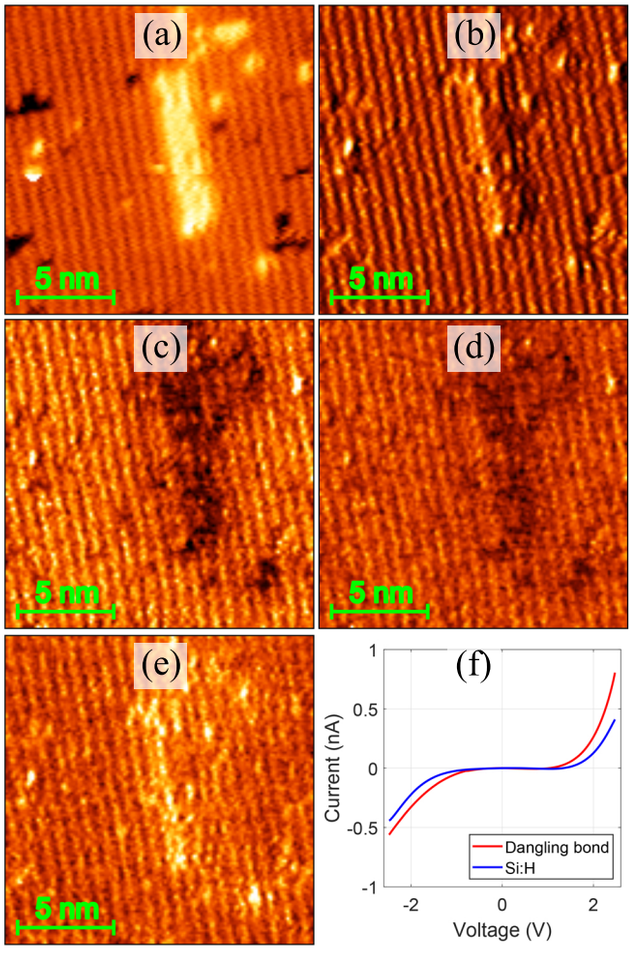

FIG. 6. Simultaneous STM and STS imaging of a Si(100)-2×1:H passivated surface. A 2 kHz sinusoidal signal with the amplitude of + 2.5 V was applied to the sample. (a) The topography image was obtained by closing the feedback loop on the a_1 signal, the in-phase component of current with the modulation. (b) a_1 image of the same area. (c), (d), and (e) The tunneling current image at the voltage of - 2.3 V, - 1.8 V, and + 2.3 V, respectively obtained form the I-V curve data of each pixel. (f) I(V) on a dangling bond (red curve) and on a Si-H bond (black curve). All of the data were obtained simultaneously.

This is equivalent to 1766 samples or 7.68 cycles per silicon atom. Higher resolution and more cycles to further reduce noise would be available at slower scan speeds. This setup enables us to acquire a tunneling current image for every sample bias voltage between -2.5 V and +2.5 V. Fig. 6 (c), (d), and (e) show the tunneling current image at the sample voltage of - 2.3 V, - 1.8 V, and + 2.3 V, respectively. Fig. 6 (f) compares the I-V curves obtained on a dangling bond (DB) and on a Si-H bond. The tunneling current at a specific voltage depends on the physical height of surface features and the local density of electron states (LDOS). We observe in Fig. 6 (e) that contrast between tunneling current on a dangling bond and on a Si-H bond at the sample voltage of + 2.3 V is more striking compared to the negative voltages in Fig. 6 (c) and (d). The smaller band gap on the dangling bond produces a larger current in this case. These measurements resemble those reported in previous studies[28–31]. For a $7.2\,nm \times 7.2\,nm$ sample area with 80 scan lines, the entire imaging/spectroscopy procedure with this method requires only 12 seconds. That is, our method constructs a spectroscopic map of the surface at least 1500 times faster than the conventional CITS method[9].

VI. CONCLUSIONS

In this work, we have developed a method that enables us to obtain dI/dV and d^2I/dV^2 images with a better accuracy than conventional methods, due to an improved SNR. By incorporating notch filters in the feedback loop of the STM control system, we were able to increase the amplitude of the modulation signal without compromising the quality of the topography signal, or running the risk of a tip crash. We introduced constant differential conductance imaging mode to produce the topography image of the surface. In this imaging mode, a modulation signal is added to the bias voltage and the in-phase component of current is kept constant throughout the experiment. This is particularly advantageous to obtain a cleaner topography image in the presence of low-frequency noise (flicker noise) in the current signal. Finally, an ultra fast spectroscopy method was proposed. This method provides an I-V spectra for every pixel of an image during scanning and significantly reduces the spectroscopy time. Unlike the conventional spectroscopy techniques, experimental requirements for our spectroscopy method are easily fulfilled at a room temperature. Furthermore, implementing this method does not require additional hardware if the lock-in amplifier is incorporated in the STM control software.

ACKNOWLEDGMENTS

This material is based upon work supported by the U.S. Department of Energy's Office of Energy Efficiency and Renewable Energy (EERE) under the Advanced Manufacturing Office Award No. DE-EE0008322.

DATA AVAILABILITY

The data that support the findings of this study are available within the article.

[1] G. Binnig, H. Rohrer, Ch. Gerber, and E. Weibel. Tunneling through a controllable vacuum gap. *Applied Physics Letters*, 40(2):178–180, 1982.
[2] G. Binnig, H. Rohrer, Ch. Gerber, and E. Weibel. 7 × 7 Reconstruction on Si(111) Resolved in Real Space. *Phys. Rev. Lett.*, 50:120–123, Jan 1983.
[3] R. M. Feenstra. Scanning tunneling spectroscopy. *Surface Science*, 299-300:965–979, 1994.

[4]J. H. G. Owen, D. R. Bowler, C. M. Goringe, K. Miki, and G. A. D. Briggs. Identification of the Si(001) missing dimer defect structure by low bias voltage STM and LDA modelling. *Surface Science*, 341(3):L1042–L1047, 1995.

[5]R. J. Hamers. Atomic-resolution surface spectroscopy with the scanning tunneling microscope. *Annual Review of Physical Chemistry*, 40(1):531–559, 1989.

[6]P. Sutter, P. Zahl, E. Sutter, and J. E. Bernard. Energy-filtered scanning tunneling microscopy using a semiconductor tip. *Physical review letters*, 90(16):166101, 2003.

[7]R. M. Feenstra, J. A. Stroscio, J. Tersoff, and A. P. Fein. Atom-selective imaging of the GaAs (110) surface. *Physical Review Letters*, 58(12):1192, 1987.

[8]R. J. Hamers, R. M. Tromp, and J. E. Demuth. Surface Electronic Structure of Si (111)-(7×7) Resolved in Real Space. *Phys. Rev. Lett.*, 56:1972–1975, May 1986.

[9]A. Belianinov, P. Ganesh, W. Lin, B. C. Sales, A. S. Sefat, S. Jesse, M. Pan, and S. V. Kalinin. Research Update: Spatially resolved mapping of electronic structure on atomic level by multivariate statistical analysis. *APL Materials*, 2(12):120701, 2014.

[10]G. Binnig, N. Garcia, and H. Rohrer. Conductivity sensitivity of inelastic scanning tunneling microscopy. *Physical Review B*, 32(2):1336–1338, 1985.

[11]J. Lambe and R. C. Jaklevic. Molecular Vibration Spectra by Inelastic Electron Tunneling. *Physical Review*, 165(3):821–832, January 1968.

[12]A. S. Hallbäck, N. Oncel, J. Huskens, H. J. Zandvliet, and B. Poelsema. Inelastic Electron Tunneling Spectroscopy on Decanethiol at Elevated Temperatures. *Nano Letters*, 4(12):2393–2395, December 2004.

[13]H. Alemansour, S. O. R. Moheimani, J. H. G. Owen, J. N. Randall, and E. Fuchs. High signal-to-noise ratio differential conductance spectroscopy. *Journal of Vacuum Science & Technology B*, 39(1):010601, 2021.

[14]H. Alemansour, S. O. R. Moheimani, J. H. G. Owen, J. N. Randall, and E. Fuchs. Controlled removal of hydrogen atoms from H-terminated silicon surfaces. *Journal of Vacuum Science & Technology B*, 38(4):040601, July 2020.

[15]Chr. Wittneven, R. Dombrowski, M. Morgenstern, and R. Wiesendanger. Scattering states of ionized dopants probed by low temperature scanning tunneling spectroscopy. *Phys. Rev. Lett.*, 81:5616–5619, Dec 1998.

[16]S. H. Tessmer, D. J. Van Harlingen, and J. W. Lyding. Integrated cryogenic scanning tunneling microscopy and sample preparation system. *Review of Scientific Instruments*, 65(9):2855–2859, 1994.

[17]`https://www.zyvexlabs.com/apm/products/zyvector/`. [Online; accessed 22-May-2021].

[18]M. C. Hersam, N. P. Guisinger, and J. W. Lyding. Silicon-based molecular nanotechnology. *Nanotechnology*, 11(2):70–76, jun 2000.

[19]J. A. Dagata, J. Schneir, H. H. Harary, C. J. Evans, M. T. Postek, and J. Bennett. Modification of hydrogen-passivated silicon by a scanning tunneling microscope operating in air. *Applied Physics Letters*, 56(20):2001–2003, 1990.

[20]J. W. Lyding, T.-C. Shen, J. S. Hubacek, J. R. Tucker, and G. C. Abeln. Nanoscale patterning and oxidation of H-passivated Si(100)-2×1 surfaces with an ultrahigh vacuum scanning tunneling microscope. *Applied Physics Letters*, 64(15):2010–2012, 1994.

[21]J. R. Tucker, C Wang, and T.-C. Shen. Metal silicide patterning: a new approach to silicon nanoelectronics. *Nanotechnology*, 7(3):275–287, sep 1996.

[22]G. P. Lopinski, D. D. M. Wayner, and R. A. Wolkow. Self-directed growth of molecular nanostructures on silicon. *Nature*, 406(6791):48–51, 2000.

[23]S. O. R. Moheimani and H. Alemansour. A new approach to removing H atoms in hydrogen depassivation lithography. In Eric M. Panning and Martha I. Sanchez, editors, *Novel Patterning Technologies for Semiconductors, MEMS/NEMS and MOEMS 2020*. SPIE, March 2020.

[24]B. Voigtländer. *Scanning Probe Microscopy*. Springer Berlin Heidelberg, 2015.

[25]S. O. R. Moheimani and H. Alemansour. Methods and devices configured to operated scanning tunneling microscopes using out-of-bandwidth frequency components added to bias voltage and related software, May 6 2021. US Patent App. 17/089,214.

[26]F. Tajaddodianfar, S. O. R. Moheimani, J. Owen, and J. N. Randall. On the effect of local barrier height in scanning tunneling microscopy: Measurement methods and control implications. *Review of Scientific Instruments*, 89(1):013701, 2018.

[27]F. Tajaddodianfar, S. O. R. Moheimani, and J. N. Randall. Scanning tunneling microscope control: A self-tuning pi controller based on online local barrier height estimation*. *IEEE Transactions on Control Systems Technology*, 27(5):2004–2015, 2019.

[28]A. Bellec, D. Riedel, G. Dujardin, O. Boudrioua, L. Chaput, L. Stauffer, and P. Sonnet. Electronic properties of the *n*-doped hydrogenated silicon (100) surface and dehydrogenated structures at 5 K. *Phys. Rev. B*, 80:245434, Dec 2009.

[29]H. Labidi, M. Taucer, M. Rashidi, M. Koleini, L. Livadaru, J. Pitters, M. Cloutier, M. Salomons, and R. A. Wolkow. Scanning tunneling spectroscopy reveals a silicon dangling bond charge state transition. *New Journal of Physics*, 17(7):073023, jul 2015.

[30]P. G. Piva, G. A. DiLabio, L. Livadaru, and R. A. Wolkow. Atom-scale surface reactivity mediated by long-ranged equilibrium charge transfer. *Phys. Rev. B*, 90:155422, Oct 2014.

[31]T. Škereň, S. A. Koester, B. Douhard, C. Fleischmann, and A. Fuhrer. Bipolar device fabrication using a scanning tunnelling microscope. *Nature Electronics*, 3(9):524–530, 2020.

Journal of Vacuum Science Technology B

PLEASE CITE THIS ARTICLE AS DOI: 10.1116/6.0001087

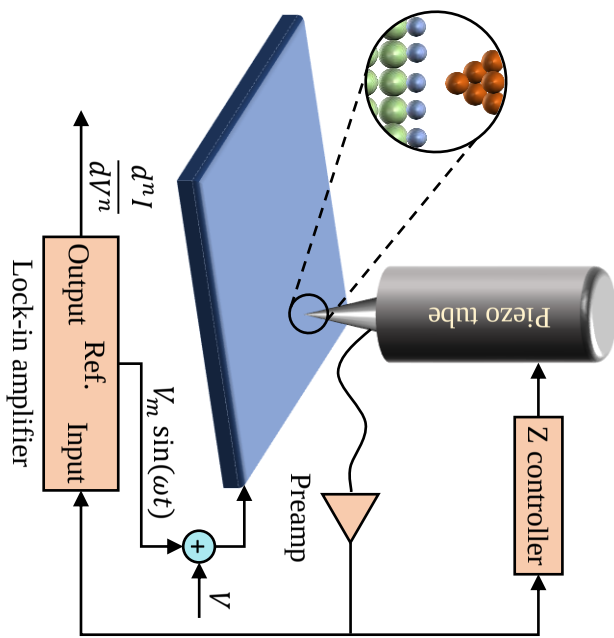

Journal of Vacuum Science Technology B

PLEASE CITE THIS ARTICLE AS DOI: 10.1116/6.0001087

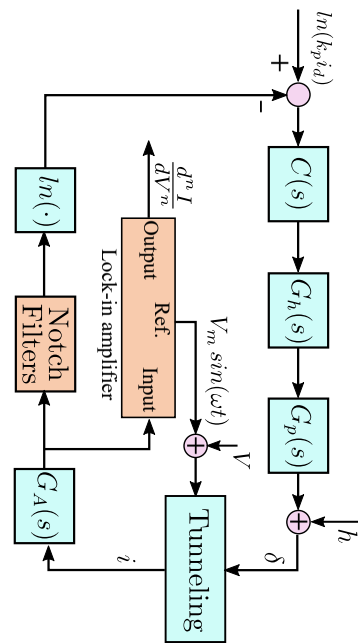

Journal of Vacuum Science Technology B

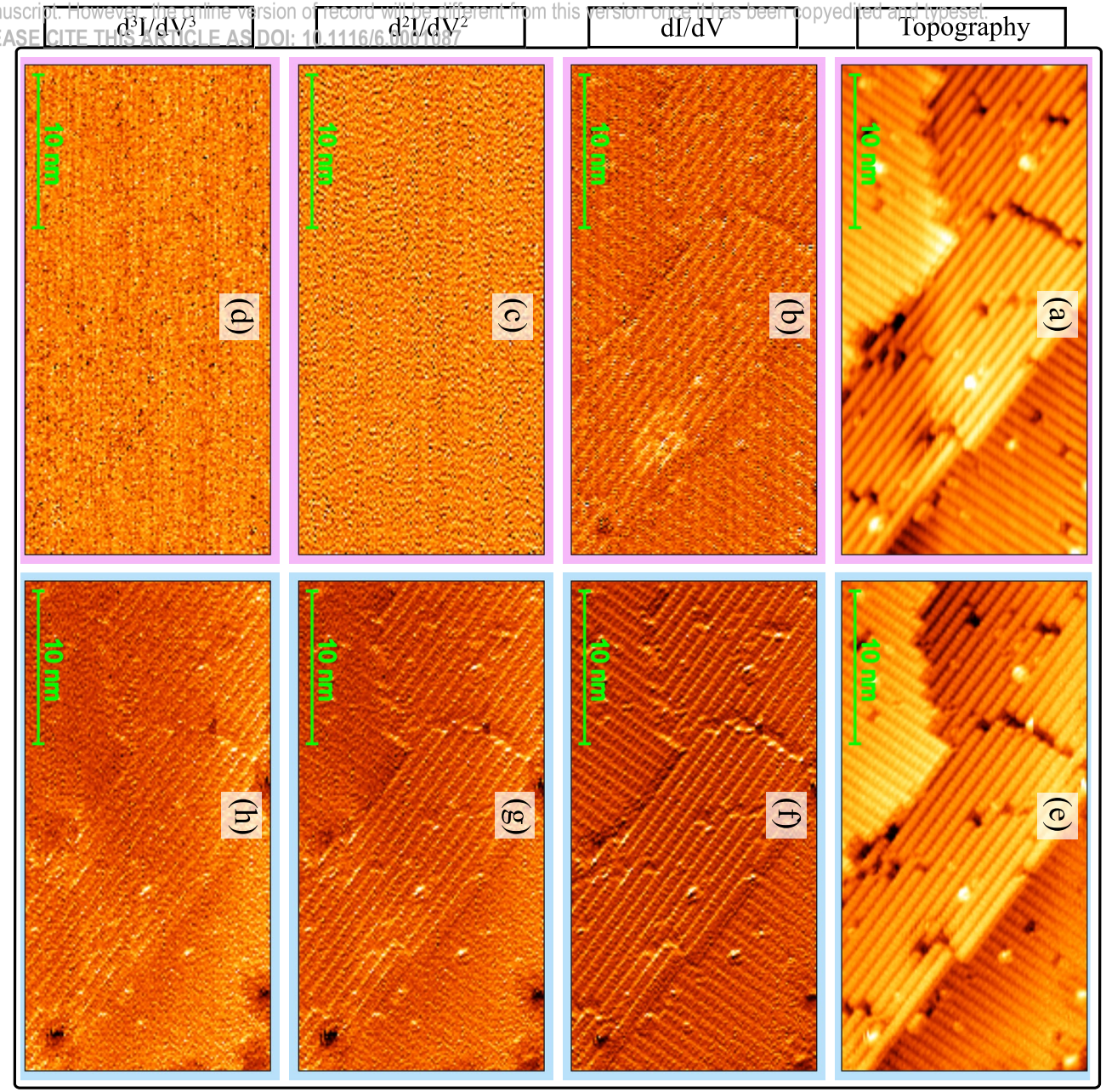

Journal of Vacuum Science Technology B

PLEASE CITE THIS ARTICLE AS DOI: 10.1116/6.0001087

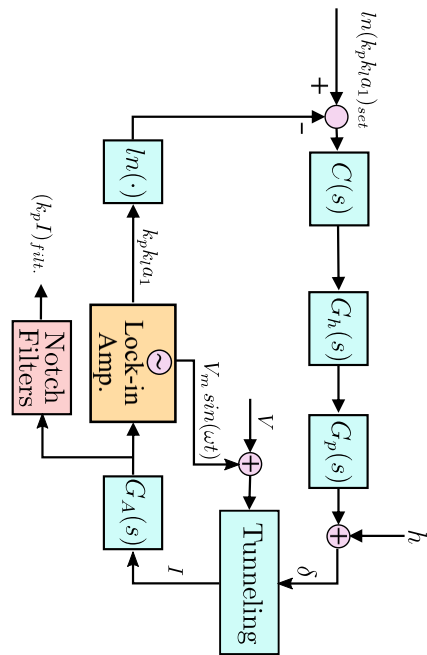

Journal of Vacuum Science Technology B

PLEASE CITE THIS ARTICLE AS DOI: 10.1116/6.0001087

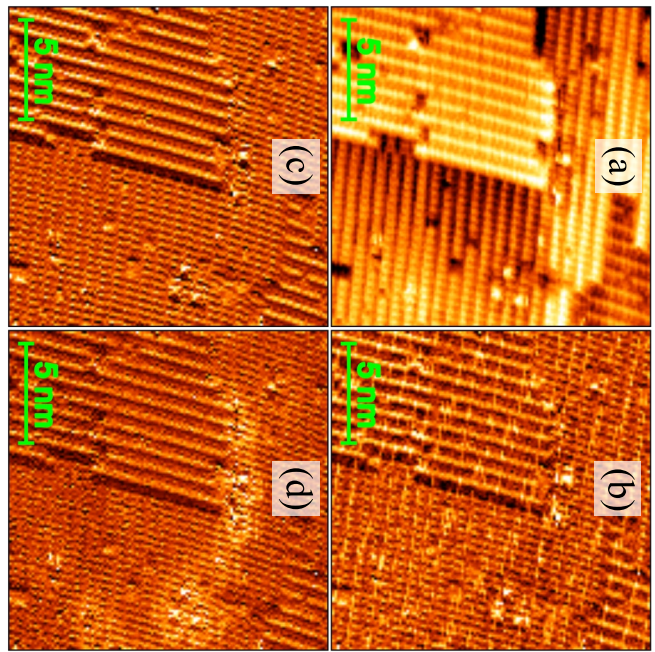

Journal of Vacuum Science Technology B

PLEASE CITE THIS ARTICLE AS DOI: 10.1116/6.0001087